

Characterization of Nonlinear Optical Properties of Crystal $\text{RbGeCl}_3 \cdot x(\text{H}_2\text{O})$ in Infrared Region

Li-Chuan Tang¹, Li-Qiang Liu², Yia-Chung Chang^{1,3}, Jui-hsien Yao¹, Jung-Yau Huang¹, and Chen-Shiung Chang^{1*}

¹Department of Photonics and Institute of Electro-Optical Engineering, National Chiao Tung University, Hsinchu 30010, Taiwan, R.O.C.

²College of Materials Science and Engineering, Shandong Jianzhu University, Jinan 250101, P. R. China

³Research Center for Applied Science, Academia Sinica, Taipei 11529, Taiwan, R.O.C.

Received March 31, 2009; accepted May 22, 2009; published online August 20, 2009

The nonlinear optical (NLO) property of hydrated rubidium germanium chloride (HRGC), $\text{RbGeCl}_3 \cdot x(\text{H}_2\text{O})$, is identified. Infrared absorption data support structural evidence that HRGC contain co-ordinated water molecules with strong hydrogen bond. The infrared spectrum indicated HRGC is transparent in most of the infrared region with only little influence from water. Calculations based on density functional theory shows that the band gap of the RbGeCl_3 (RGC) crystal is at least 3.84 eV, which is larger than that of the infrared (IR) NLO crystal CsGeCl_3 . Single crystals of HRGC, sized up to $3 \times 2 \times 1 \text{ cm}^3$, were grown in aqueous solution by a slow dehydrate technique. The synthetic, structural, and optical properties of an off-centrosymmetric IR nonlinear optical (NLO) $\text{RbGeCl}_3 \cdot x(\text{H}_2\text{O})$ crystal were investigated experimentally. Powder second harmonic generation (PSHG) measurement indicates that the crystal structure of HRGC becomes off-centrosymmetric. Precise X-ray diffraction measurements showed that [100] family diffraction peaks split slightly. Unlike the RGC crystal structure whose space group is $P2_1\bar{m}$, the HRGC crystal loses the inversion symmetry. Comparisons with known NLO material KH_2PO_4 (KDP), indicate that HRGC's NLO susceptibility, $\chi^{(2)}$, is about one third of that for KDP. The absorption edge of HRGC occurred at 310 nm ($\approx 4.0 \text{ eV}$), which indicates NLO HRGC crystal can have larger laser damage threshold. According to the Fourier transform infrared (FTIR) measurement, HRGC has a transparent region from 0.31 to 30 μm , thus it can be applied to wider optical spectrum from ultraviolet, visible, to mid-IR. © 2009 The Japan Society of Applied Physics

DOI: 10.1143/JJAP.48.082001

1. Introduction

The second-order nonlinear optical (NLO) materials play a key role in the field of optics such as laser frequency conversion and optical parametric oscillation/amplification (OPO/OPA).¹ For inorganic second-order NLO materials, several crystals used in ultraviolet (UV) and visible (vis) regions were proposed in the past two decades, e.g., KH_2PO_4 (KDP), KTiOPO_4 (KTP), $\beta\text{-BaB}_2\text{O}_4$ (BBO), LiB_3O_5 (LBO), etc. But in the infrared (IR) region the current materials, such as AgGaSe_2 , ZnGeP_2 , are not good enough for applications, mainly due to their low laser damage threshold, as their band gaps are narrow. So the search for new NLO materials in IR region becomes one of the most important challenges due to their potentially wide applications in fields such as laser technology and molecular spectroscopy.²

Up to now, several ternary halides were discovered to exhibit second-order NLO properties, such as ABX_3 ($A = \text{Cs, Rb, B} = \text{Ge, Cd, X} = \text{Cl, Br, I}$).³⁻⁵ CsGeCl_3 (cesium germanium chloride, CGC), which was found to possess excellent second-order NLO properties, exhibits a second-harmonic generation (SHG) five times larger than that of KDP. Furthermore, its damage threshold reaches 200 MW/cm^2 .⁶ In order to get materials with high laser damage threshold, some halide compounds, e.g., CGC were excellent choices because of their large band gaps, which will be beneficial to the improvement of the laser damage threshold. CGC was announced to be an innovative nonlinear IR crystal by Ewbank *et al.*⁵ and Gu *et al.*⁶⁻⁸ Recently, more ternary halides with perovskite structure, ABX_3 ($A = \text{Cs, Rb, B} = \text{Ge, Cd, X} = \text{Cl, Br, I}$) became a new category of nonlinear optical materials, with potential application from visible to infrared. These NLO applications include difference-frequency mixing, optical parametric generation and

amplification. The electronic and linear optical properties of CsGeI_3 were also reported by Tang *et al.*⁹ CsCdBr_3 was found to be noncentrosymmetric, i.e., lack of inversion symmetry, by Ren *et al.*¹⁰ At the same time, Ren *et al.* also reported a structure-tuned ternary halide, i.e., $\text{RbCdI}_3 \cdot x\text{H}_2\text{O}$ (rubidium cadmium iodide monohydrate, RCIM),¹¹ which showed sizable second-order NLO effects. Similar to RCIM, HRGC [$\text{RbGeCl}_3 \cdot x(\text{H}_2\text{O})$, with $0.0 \leq x \leq 0.2$] also possesses strong NLO effects, which are examined in this work.

One of the continued challenges in ternary halides concerns the elucidation of structure-property relationships. Nowhere is this more true than the second-order nonlinear optical (NLO) properties, i.e., SHG properties. Viable SHG materials must possess the following attributes: transparency in the relevant wavelengths, ability to withstand laser irradiation, and chemical stability. Most importantly, the material in question must be crystallographically noncentrosymmetric (NSC). Mathematically it has been known for some time that only an NSC arrangement of atoms may produce a second-order NLO response.¹²

In this paper, the synthesis and powder SHG behavior of $\text{RbGeCl}_3 \cdot x(\text{H}_2\text{O})$ are reported. Through these powder measurements, an approximate value for $d_{\text{effect}}^{2\omega}$, the NLO bond susceptibility is evaluated.

2. Experiments

Certain geometric (e.g., second-order Jahn–Teller, SOJT) distortions¹³⁻¹⁹ were concerned with structural changes attributed to a nondegenerate ground state, interacting with a low-lying excited state. The distortion occurs where the energy gap between the highest occupied and lowest unoccupied molecular orbitals (HOMO/LUMO) is small and there is a symmetry-allowed distortion permitting the mixing of the HOMO and LUMO states. With perovskite-type ternary oxides as well as halides ABX_3 ($A = \text{Cs, Rb, B} = \text{Ge, Cd, X} = \text{Cl, Br, I}$), Goldschmidt's tolerance factor

*E-mail address: newton4538.eo85g@nctu.edu.tw

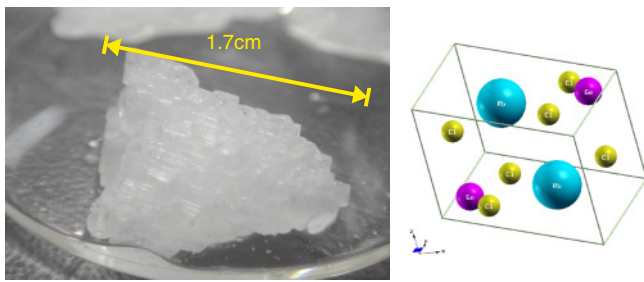


Fig. 1. (Color online) One of the as-grown $\text{RbGeCl}_3 \cdot x(\text{H}_2\text{O})$ crystals and the crystal structure model of the monoclinic RbGeCl_3 crystal, whose space group is $P2_1\bar{m}$.

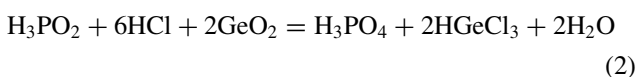
$t^{(20,21)}$ serves as a discriminating parameter of classifying perovskites in terms of structure modifications and the resulting physical properties.^{22–26} The type of stacking depends on the tolerance factor $t^{(20,21)}$

$$t = \frac{r_A + r_X}{\sqrt{2} \cdot (r_B + r_X)}, \quad (1)$$

where subscripts A and B denote the large and small cation, respectively and X denotes the anion. r denotes the ionic radii of Shannon and Prewitt^{27,28} which depend on the coordination number and bonding-specimens. The tolerance factor t of the RbGeCl_3 crystal structure is about 0.92 and far from the ideal value, 1.0. The t -ratio of RbGeCl_3 and CsGeCl_3 is similar to that of SrTiO_3 and BaTiO_3 . RbGeCl_3 can be considered as a substitutional material for CsGeCl_3 and their mixture can be used to tune the electronic or optical properties. The RbGeCl_3 crystal belongs to a monoclinic space group $P2_1\bar{m}$, ($a = 7.988 \text{ \AA}$, $b = 6.941 \text{ \AA}$, $c = 5.800 \text{ \AA}$, $\alpha = \gamma = 90^\circ$, $\beta = 106.340^\circ$),^{29,30} which can be considered as highly distorted perovskite crystal structure of CsGeCl_3 , as shown in Fig. 1.

2.1 Synthesis

The synthetic procedure is illustrated in Fig. 2, which is modified from the work of Gu and coworkers.^{6–8} Christensen *et al.*³¹ and Tananaev *et al.*³² used different synthesis methods, but their methods were complex and the productivity was poor. We adopted the modified method for synthesizing $\text{RbGeCl}_3 \cdot x(\text{H}_2\text{O})$. 25 ml of 50% H_3PO_2 , 25 ml of 37.5% HCl and 5 g of GeO_2 were loaded into a 500 ml beaker, and then heated to 85–90 °C. The solution was vigorously mixed for 5 h then cooled to room temperature. After removing the precipitate, 6.05 g RbCl was added and the temperature raised to the boiling point, then the mixture was cooled to room temperature again. A white precipitation was formed. The reaction equations are as follows:



and



Recrystallization is achieved via mixing the precipitation RbGeCl_3 with 1 : 1 concentrated HCl and alcohol solution and we can obtain colorless $\text{RbGeCl}_3 \cdot x(\text{H}_2\text{O})$ crystals.

HRGC is synthesized by a similar procedure, as reported by Nyqvist *et al.*³³ The synthesis is carried out in an

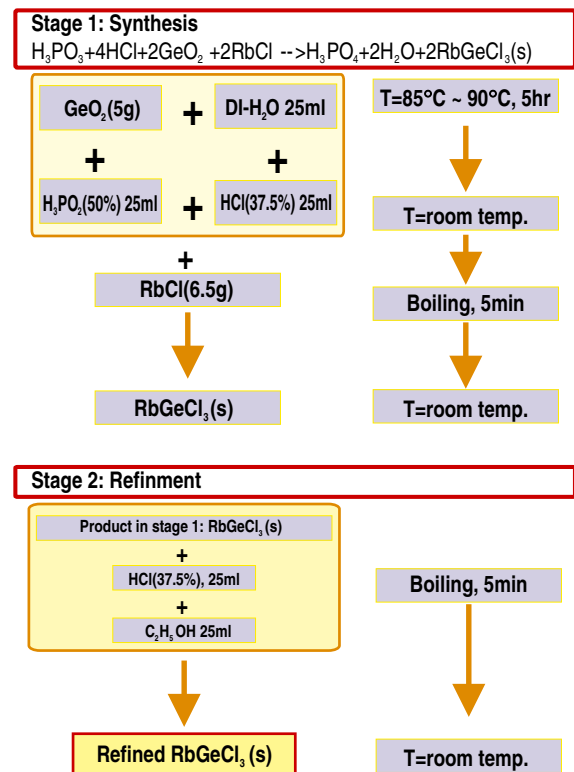


Fig. 2. (Color online) The synthesis procedure of monoclinic non-linear optical crystal HRGC.

aqueous solution under normal condition. Analytical pure RbCl and GeCl_2 (with mole ratio 1 : 1) were dissolved in a certain amount of hot distilled water, and colorless crystals were separated out during cooling. Crystal is grown by utilizing a solvent slow evaporation technique in an aqueous solution. The size of the single crystal reached $3 \times 2 \times 1 \text{ cm}^3$ (see Fig. 1).

2.2 X-ray diffraction

The X-ray single crystal structure analysis is used to confirm the structure of the product. A single crystal with dimensions of $1.10 \times 0.80 \times 0.40 \text{ mm}^3$ is mounted on a Enraf-Nonius CAD4 diffractometer using a graphite-monochromated $\text{Cu K}\alpha$ ($\lambda = 1.542 \text{ \AA}$) radiation. The data were collected at room temperature using the $\omega/2\theta$ scan mode and corrected for Lorentz and polarization effects as well as the absorption during data reduction using Enraf-Nonius Molenv/VAX software.

Although the structure of HRGC has been reported,^{29,30} we felt it important to determine the structure to better understand the SHG properties. Our data confirm that HRGC crystallizes in the noncentrosymmetric rhombohedral space group $P2_1\bar{m}$ (No. 11) with $a = 7.988 \text{ \AA}$, $b = 6.941 \text{ \AA}$, $c = 5.800 \text{ \AA}$, $\alpha = \gamma = 90.0^\circ$, and $\beta = 106.34^\circ$. The cell parameters estimated from the first-principles calculation based on the WIEN2k³⁴ package are $a = 8.375 \text{ \AA}$, $b = 7.141 \text{ \AA}$, $c = 5.918 \text{ \AA}$, $\alpha = \gamma = 90.0^\circ$, and $\beta = 107.24^\circ$, which compare well with the single-crystal data.

2.3 Thermogravimetric measurements

The thermo-gravimetric analysis (TGA) measurement in static air was performed on a Shimadzu DT-40 at a scan rate

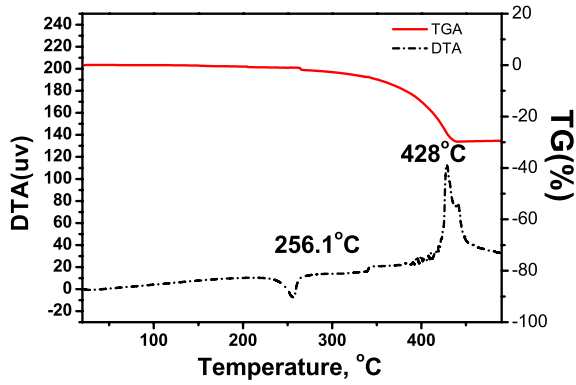


Fig. 3. (Color online) The thermal analysis of monoclinic nonlinear optical crystal HRGC.

of 20 °C/min. By using DTA1700 high temperature analysis instrument, thermal properties were measured.

The resulted curve of TGA/DTA measurements on HRGC powder (Fig. 3) reveals one transition in the range of 250–260 °C, corresponding to a weight loss about 1.093%, which is in agreement with the calculated weight loss of water. The main weight loss occurred at temperature above 400 °C.

2.4 Transmittance spectrum

Because wide transparent range is a crucial consideration for developing innovative NLO crystals used in IR range. The UV–vis electronic absorption spectra of HRGC were performed on a Hitachi 3400 UV–vis spectrophotometer. The infrared spectrum was recorded on a NICOLET 170SX Fourier-transform infrared (FTIR) spectrophotometer with KBr pellet from 4000 to 400 cm⁻¹. The HRGC transparent spectrum measurement was prepared by using HRGC solvent and HRGC as a pressed powder tablet. Then, the far-IR limitation of HRGC was detected by its Raman peaks.

2.5 Second-order nonlinear optical measurements

Powder SHG measurements, which were reported by Chen *et al.*,³⁵⁾ were performed on a modified Kurtz-NLO³⁶⁾ system using 1064 nm light (Fig. 4). A continuum Minilite II laser, operating at 1 Hz, is used for all measurements. The average energy of laser pulse is 3 mJ. Since the SHG efficiency of powders has been shown to depend strongly on particle size,^{36,37)} polycrystalline HRGC is ground and sieved (Newark Wire Cloth) into distinct particle size ranges, ≤20 μm, 20 to 45 μm, 45 to 63 μm, 63 to 75 μm, 75 to 90 μm, 90 to 125 μm, and 125 to 138 μm. To make relevant comparison with known SHG materials, crystalline KDP is also ground and sieved into the same particle-size ranges. All of the powders were placed in separate capillary tubes. The SHG, i.e., 532 nm green light, radiation is collected in reflection and detected by a photomultiplier tube (Oriel Instruments). To detect only the SHG light, a 532 nm narrow-band-pass interference filter is attached to the tube. A digital oscilloscope (Tektronix TDS 302) is used to view the SHG signal.

Considering a normally incident beam with wavelength λ on a crystal plate with thickness L , the total second-harmonic intensity can be expressed as³⁸⁾

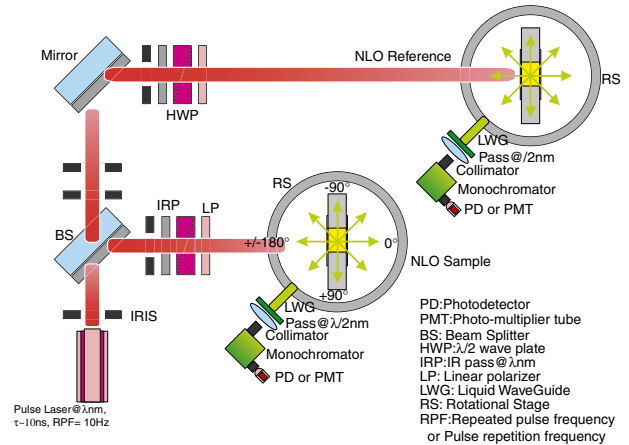


Fig. 4. (Color online) Experimental setup used for measuring the second harmonic scattering pattern from a crystalline powder sample.

$$I_{2\omega} = \frac{128\pi^5 d_{\text{eff}}^2 I_{\omega}^2 L^2 \sin^2(\Delta k L/2)}{n_{\omega}^2 n_{2\omega} \lambda_{2\omega}^2 c (\Delta k L/2)^2}, \quad (4)$$

where $\Delta k = k(2\omega) - 2k(\omega)$, I_{ω} is the intensity of the incident fundamental beam, n_{ω} , $n_{2\omega}$, and d_{eff} are the indices of refraction and the effective nonlinearity of the crystal plate. When the plate is made with crystalline powders, the second-harmonic intensity becomes³⁹⁾

$$I_{2\omega} = \frac{512\pi^3 I_{\omega}^2 \bar{l}_c^2}{n_{\omega}^2 n_{2\omega} \lambda_{2\omega}^2 c} \langle d_{\text{eff}}^2 \rangle \frac{L}{r} \sin^2 \left[\frac{\pi}{2} \left(\frac{\bar{r}}{\bar{l}_c} \right) \right]. \quad (5)$$

Here \bar{r} denotes the averaged particle size,

$$\bar{l}_c = \langle \lambda_{\omega} / 4(n_{2\omega} - n_{\omega}) \rangle \quad (6)$$

is the coherent length, and $\langle d_{\text{eff}}^2 \rangle$, the square of the effective nonlinearity averaged over the orientation distribution of crystalline powders. When the second-harmonic generation is not phase matchable, eq. (5) leads to the following asymptotic forms:³⁹⁾

$$I_{2\omega} \rightarrow \begin{cases} \frac{256\pi^3 I_{\omega}^2 \bar{l}_c^2}{n_{\omega}^2 n_{2\omega} \lambda_{2\omega}^2 c} (L/\bar{r}) \langle d_{\text{eff}}^2 \rangle, & \leftarrow \bar{r} \gg \bar{l}_c \\ \frac{128\pi^5 I_{\omega}^2}{n_{\omega}^2 n_{2\omega} \lambda_{2\omega}^2 c} L \bar{r} \langle d_{\text{eff}}^2 \rangle, & \leftarrow \bar{r} \ll \bar{l}_c \end{cases}. \quad (7)$$

If the second-harmonic generation satisfies the type-I phase matching condition, we can rewrite eq. (4) as⁴⁰⁾

$$I_{2\omega}(\bar{r}, \theta) = \frac{128\pi^5 I_{\omega}^2}{n_{\omega}^2 n_{2\omega} \lambda_{2\omega}^2 c} L \cdot \bar{r} \langle d_{\text{eff}}^2 \rangle \frac{\sin^2 \left[\frac{\pi}{2} \frac{\bar{r}}{\bar{l}_{\text{pm}}} (\theta - \theta_{\text{pm}}) \right]}{\left[\frac{\pi}{2} \frac{\bar{r}}{\bar{l}_{\text{pm}}} (\theta - \theta_{\text{pm}}) \right]}, \quad (8)$$

where

$$\bar{l}_{\text{pm}} = \lambda / (4|\Delta n_{\text{B},2\omega}| \sin 2\theta_{\text{pm}}), \quad (9)$$

and θ_{pm} is the phase matching angle. Here $\Delta n_{\text{B},2\omega} = n_{\text{E},2\omega} - n_{\text{O},2\omega}$ denotes the birefringence of material at the second-harmonic wavelength. In the event that $\bar{r} \gg \bar{l}_{\text{pm}}$ or $\bar{r} \ll \bar{l}_{\text{pm}}$, eq. (8) can be simplified to

$$I_{2\omega} \rightarrow \begin{cases} \frac{256\pi^4 I_{\omega}^2}{n_{\omega}^2 n_{2\omega} \lambda_{2\omega}^2 c} L \bar{l}_{\text{pm}} \langle d_{\text{eff}}^2 \rangle, & \leftarrow \bar{r} \gg \bar{l}_{\text{pm}} \\ \frac{128\pi^5 I_{\omega}^2}{n_{\omega}^2 n_{2\omega} \lambda_{2\omega}^2 c} L \bar{r} \langle d_{\text{eff}}^2 \rangle, & \leftarrow \bar{r} \ll \bar{l}_{\text{pm}} \end{cases}. \quad (10)$$

Chen *et al.*³⁵⁾ derived a useful empirical formula, which possesses the correct asymptotic forms in eq. (10), to depict the overall variation in second harmonic intensity with particle size \bar{r}

$$I_{2\omega} = I_0 \sqrt{1 - \exp[-(\bar{r}/A)^2]} \quad (11)$$

with

$$I_0 = \frac{256\pi^4 I_\omega^2}{n_\omega^2 n_{2\omega} \lambda_{2\omega}^2 c} L \bar{l}_{\text{pm}} \langle d_{\text{eff}}^2 \rangle \quad (12)$$

and

$$A \approx 9 \bar{l}_{\text{pm}}. \quad (13)$$

An experimental arrangement for measuring the second harmonic scattering pattern from crystalline powders is described in Fig. 4. In this setup, a normally incident beam is shed on the sample cell. A liquid light guide with its input end attached to a rotation stage is employed to collect the second harmonic intensity at various scattering angles. We can integrate the second harmonic pattern over scattering angle to yield the total second harmonic intensity, $I_{2\omega}$. The second harmonic pattern over scattering angle to yield the total second harmonic intensity, $I_{2\omega}$, was integrated. The square of the effective nonlinearity, $\langle d_{\text{eff}}^2 \rangle$, averaged over the orientation distribution of crystalline powders of HRGC was determined by

$$\begin{aligned} \langle d_{\text{eff}}^2 \rangle_{\text{HRGC}} &= \langle d_{\text{eff}}^2 \rangle_{\text{KDP}} \frac{I_{2\omega, \text{HRGC}}^{\text{total}} n_{\omega, \text{HRGC}}^2 n_{2\omega, \text{HRGC}}}{I_{2\omega, \text{KDP}}^{\text{total}} n_{\omega, \text{KDP}}^2 n_{2\omega, \text{KDP}}} \\ &\approx \langle d_{\text{eff}}^2 \rangle_{\text{KDP}} \frac{I_{2\omega, \text{HRGC}}^{\text{total}} n_{\text{HRGC}}^3}{I_{2\omega, \text{KDP}}^{\text{total}} n_{\text{KDP}}^3} \end{aligned} \quad (14)$$

with a reference NLO crystal, e.g., KDP, when $n \approx n_\omega \approx n_{2\omega}$.

3. Results and Discussion

Because the structure of RbGeCl₃ has been published, only a brief description will be given here, and will be compared to our measurements of HRGC.

3.1 Crystal structure and mechanical properties

Figure 5 shows the X-ray powder diffraction of the crystal HRGC. Each important peak has been labeled on the measured X-ray diffraction (XRD) patterns, e.g., the [111] plane around $2\theta \approx 20.78^\circ$ or [310] plane about $2\theta \approx 37.40^\circ$. These peaks are slightly shifted from ideal RGC diffraction pattern. From the crystal models used in this study, the water molecules are located between these atomic planes. The water molecules causes the change of interplanar spacing. The peak from [310] planes is found to achieve a minimum peak height when the water of crystallization is 50% occupied ($x \approx 0.1$). The water molecules randomly occupy the crystallographic sites between the [310] planes and cause a reduction in structural factor. The lattice parameters of RbGeCl₃·*x*(H₂O) crystals vary linearly with the amount of water.

From the first-principles calculations based on the WIEN2k package, the equation-of-state parameters such as the bulk modulus and its pressure derivative can be deduced. The bulk modulus for RbGeCl₃·*x*(H₂O) is about 9.11 GPa.

The HRGC crystal belongs to a monoclinic space group $P2_1\bar{m}$ (No. 11) with $a = 7.988 \text{ \AA}$, $b = 6.941 \text{ \AA}$, $c = 5.800 \text{ \AA}$, $\alpha = \gamma = 90.0^\circ$, and $\beta = 106.34^\circ$. Figure 1 shows the crystal

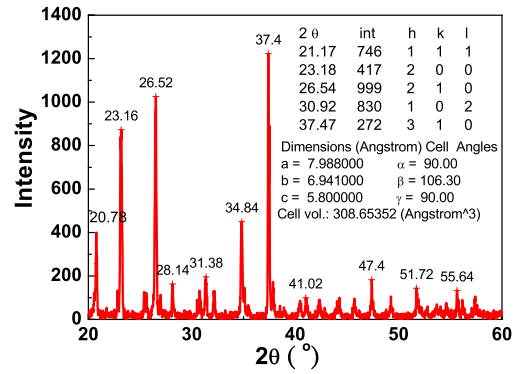


Fig. 5. (Color online) X-ray powder diffraction of the crystal HRGC. It is shown that the XRD peaks shift from that of RGC. A major peak height at [310] is observed in the NLO crystals HRGC.

packing along *a* and *c* directions. Three chloride atoms are bonded to a germanium atom to form a tetrahedron, and two such tetrahedrons are inversely mapped to each other in the primitive cell.

The germanium–chloride tetrahedrons form chain-like rows, which are parallel to one other, while rubidium atoms and water molecules are arranged between the germanium–chlorides chains. Each rubidium or water molecule is surrounded by three parallel germanium–chlorides chains. The bond length analysis showed that the bond lengths of germanium with two dangling chloride atoms, Ge–Cl(1) and Ge–Cl(2), were 2.722(3) and 2.738(3) Å, respectively, while the bond lengths of germanium with two bridging chloride atoms, Ge–Cl(3) and Ge–Cl(4), were 2.823(3) and 2.830(4) Å, respectively. So there is a distortion within one germanium–chlorides tetrahedron. Furthermore, the connecting ways of the germanium–chlorides tetrahedrons were similar, as the bridging chloride atoms were all located “below” germanium atoms, while the two dangling chloride atoms within one tetrahedron were located “above” germanium atoms as shown in Fig. 1. This means that the distortion directions of all tetrahedrons are similar. This packing mode is favorable for the accumulation of microscopic second-order NLO coefficient and leads to a relatively strong bulk NLO effect.

3.2 Second-order nonlinear optical susceptibilities

The optical SHG effect is investigated using a Kurtz powder technique. A Nd:YAG laser is utilized to generate fundamental 1064 nm light. Microcrystalline KDP served as the standard. The Kurtz powder SHG measurement showed that the intensity of double frequency signal is about one third as large as that of KDP which are 0.14 and 0.38 pm/V for HRGC and KDP,⁴¹⁾ respectively. This result is in agreement with the above analysis of the molecular structure of HRGC.

The NLO coefficient for HRGC powder is compared with KDP using a semiquantitative methods, as illustrated in §2.5. A 1.064 μm laser is split into two parts to irradiate the HRGC powder tablets and the KDP reference powder tablets. The SHG results for HRGC are about one third time as large as that of KDP references at 1.064 μm, and the damage threshold is greater than 200 MW/cm² which is similar to that of CsGeCl₃.⁷⁾

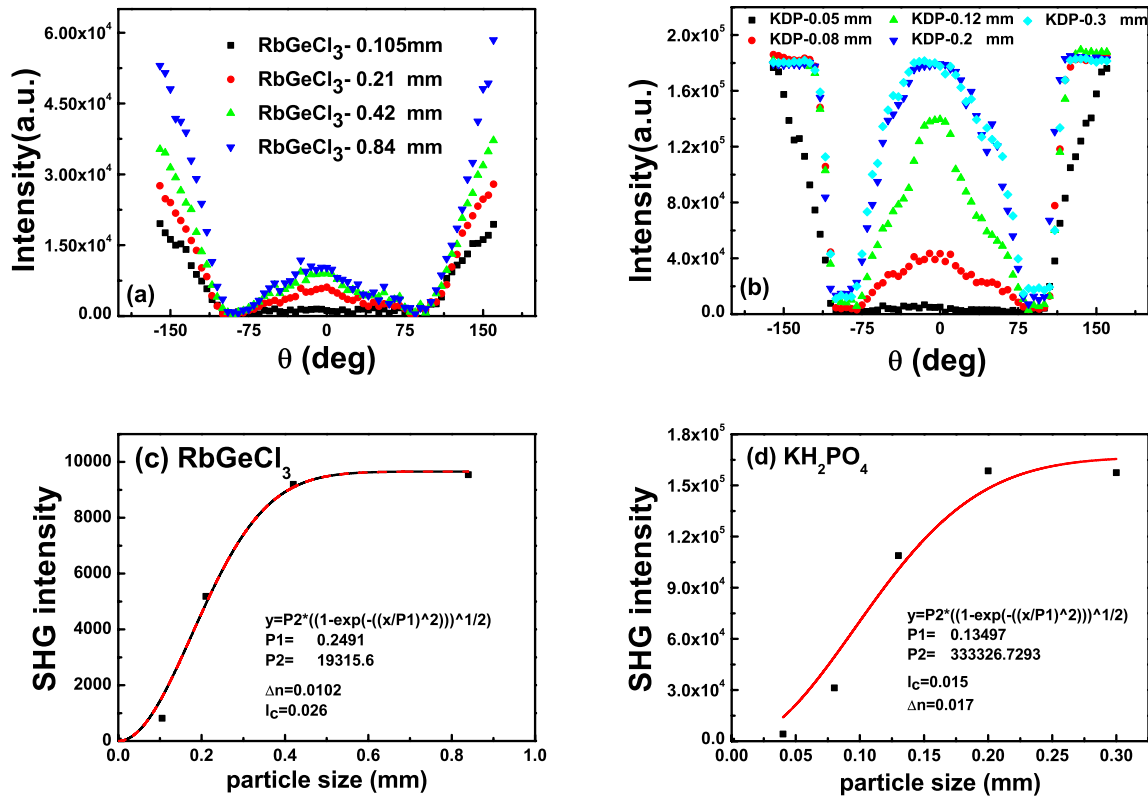


Fig. 6. (Color online) Analysis of hydradizayion contribution in the NLO crystals the second-harmonic susceptibility $\chi^{(2)}$ and the scaled values of $\chi^{(2)}$ of the NLO crystals $\text{RbGeCl}_3 \cdot \text{H}_2\text{O}$.

The Kurtz powder SHG measurement shows that the intensity of double frequency signal is about one third as large as that of KDP. This result is in agreement with above analysis of the molecular structure of HRGC. It is well known that second-order nonlinear optical susceptibility is much more sensitive to crystal structure than the linear optical susceptibility. The second-order nonlinear susceptibilities can be estimated according to eq. (14) in order to learn more about the hydrate-induced distortion. The value of $d^2 (= 2\chi^{(2)})$ is estimated to be 0.14 pm/V.

Powder SHG measurements on sieved polycrystalline HRGC revealed a less SHG efficiency 300 times that of KDP. In addition, the material is phase-matchable (see Fig. 6). That is, as the particle size becomes substantially larger than the the coherence length of the crystal, the collected SHG intensity gains no more and saturates at a certain value. Our experimental results also revealed that HRGC is damaged under prolonged laser irradiation. The capillary tube became dark after several laser shots. This phenomenon did not occur when the tube is empty. On the basis of the intensity ratio between a phase-matchable material and KDP (which is also phase-matchable), one can calculate the average NLO bond susceptibility,³⁶⁾ For phase-matchable materials, the intensity ratio can be obtained.³⁶⁾ The coherence length L_c is 20 μm for KDP and is assumed to be 15 μm for HRGC, whereas the average particle size \bar{r} is taken to be 50 μm for both materials.³⁶⁾

3.3 Transmittance spectrum

According to the first-principles calculation result, the RbGeCl_3 crystal has a direct band gap (see Fig. 7) with potential applications as efficient absorber or photon emitter.

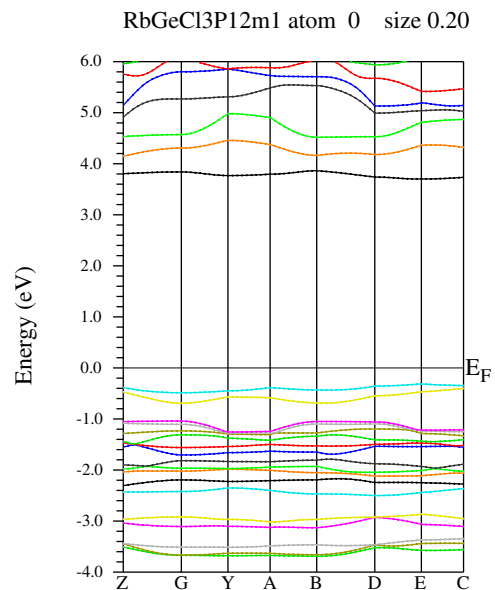


Fig. 7. (Color online) Electronic band structure of the crystals RbGeCl_3 .

To gain more insight into the calculated optical properties, we further studied the PDOS and LDOS spectra of these crystals. The calculated PDOS for RbGeCl_3 are presented in Fig. 8. Based on Fig. 8, the HOMO/LUMO values depend on the contributions of the germaniums and the chlorines.

Furthermore, in Fig. 9(a), absorption spectrum measured on single crystal $\text{RbGeCl}_3 \cdot x(\text{H}_2\text{O})$ in visible range is shown. The absorption edge is 3.84 eV. The resulting bandgap of $\text{RbGeCl}_3 \cdot x(\text{H}_2\text{O})$ can be tuned linearly in a wide spectral

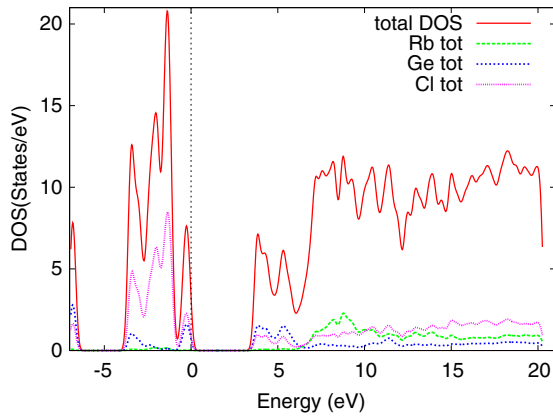


Fig. 8. (Color online) The density of state analysis contribution in the crystals RbGeCl₃.

range by adjusting the substitution composition. From the UV-vis-near IR spectrum of HRGC [Fig. 9(a)], it is transparent in the visible region and even extended to about 350 nm, which is the absorption edge of HRGC. According to these data, the band gap of the HRGC is estimated to be 4 eV, which is even larger than the band gap of the famous LiNbO₃ (3.5 eV) crystal. The band gap is related to the laser damage threshold. The larger the band gap exists, the higher the laser damage threshold is. So, the HRGC is expected to have high laser damage threshold.

The FTIR spectrum of HRGC crystalline powder is shown in Fig. 9(b). The transmittance is higher than 90% ranged from 2.5 to 25 μm. There were few absorption peaks at 2.5–2.7 μm, 3.0–5.9 μm belong to the symmetric- and asymmetric-stretching of the crystalline water. So the transparent range of HRGC were from 2.0–20 μm.

The Raman spectrum of HRGC crystalline powder is shown in Fig. 9(c). The peaks at 324.28, 278.02, 251.72, 175.50, and 124.88 cm⁻¹ are due to the stretching of the 3-fold bonds in the Ge-Cl₃⁻ cluster and the A-site cation vibration. There are no other peaks in the region. So the transparent region of HRGC is wide (from 0.31 to 30.84 μm). This is of vital importance to many applied realms such as scout and other civil applications.

4. Conclusions

In summary, hydrated rubidium Germanium chloride has been synthesized. Its single crystal with size of 3 × 2 × 1 cm³ is grown by slow evaporation in aqueous solution. The intensity of second harmonic generation effect is about one third of that of KDP, and is also phase-matchable. Infrared spectra, absorption-edge and Raman measurements indicat that the RbGeCl₃·xH₂O crystal (HRGC) is transparent in most of the IR region, and the transparent region ranges from 0.31 to 30.84 μm. The HRGC's band gap is estimated to be 3.84 eV. These results shows that HRGC can potentially be used as a new NLO crystal in the IR region.

Acknowledgments

The authors are indebted to the financial support from the National Science Council of the Republic of China under grant NSC 97-2112-M-009-013.

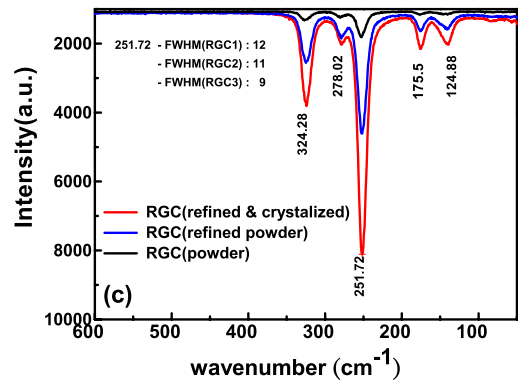
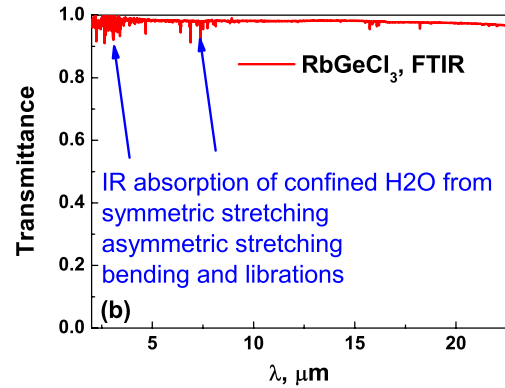
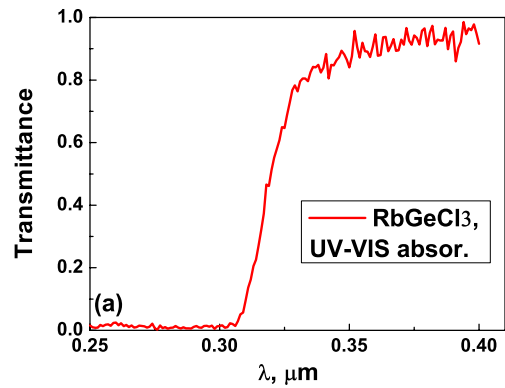


Fig. 9. (Color online) (a) Measured transmittance of the crystal RbGeCl₃·x(H₂O). (b) The measured FTIR of the crystal RbGeCl₃·x(H₂O). (c) The measured Raman spectra the crystal RbGeCl₃·x(H₂O).

- 1) J. A. Giordmaine and R. C. Miller: *Phys. Rev. Lett.* **14** (1965) 973.
- 2) V. G. Dmitriev, G. G. Gurzadyan, and D. N. Nikogosyan: *Handbook of Nonlinear Optical Crystals* (Springer, Berlin, 1999) 3rd ed.
- 3) J. Zhang, N. Su, C. Yang, J. Qin, N. Ye, B. Wu, and C. Chen: *Proc. SPIE* **3556** (1998) 1.
- 4) J. Zhang: Ph. D. thesis, Wuhan University, Department of Material Science (1995).
- 5) M. D. Ewbank, F. Cunningham, R. Borwick, M. J. Rosker, and P. Gunter: CLEO'97, 1997, paper CFA7, p. 462.
- 6) Q. Gu, Q. Pan, X. Wu, W. Shi, and C. Fang: *J. Cryst. Growth* **212** (2000) 605.
- 7) Q. Gu, Q. Pan, W. Shi, X. Sun, and C. Fang: *Prog. Cryst. Growth Charact. Mater.* **40** (2000) 89.
- 8) Q. Gu, C. Fang, W. Shi, X. Wu, and Q. Pan: *J. Cryst. Growth* **225** (2001) 501.
- 9) L.-C. Tang, C.-S. Chang, and J. Y. Huang: *J. Phys.: Condens. Matter* **12** (2000) 9129.
- 10) P. Ren, J. Qin, and C. Chen: *Inorg. Chem.* **42** (2003) 8.
- 11) P. Ren, J. Qin, T. Liu, Y. Wu, and C. Chen: *Opt. Mater.* **23** (2003) 331.

- 12) J. F. Nye: *Physical Properties of Crystals* (Oxford University Press, Oxford, U.K., 1957).
- 13) U. Opik and M. H. L. Pryce: *Proc. R. Soc. London, Ser. A* **238** (1957) 425.
- 14) R. F. W. Bader: *Mol. Phys.* **3** (1960) 137.
- 15) R. F. W. Bader: *Can. J. Chem.* **40** (1962) 1164.
- 16) R. G. Pearson: *J. Am. Chem. Soc.* **91** (1969) 4947.
- 17) R. G. Pearson: *Mol. Struct.: THEOCHEM* **103** (1983) 25.
- 18) R. A. Wheeler, M.-H. Whangbo, T. Hughbanks, R. Hoffmann, J. K. Burdett, and T. A. J. Albright: *J. Am. Chem. Soc.* **108** (1986) 2222.
- 19) M. Kunz and I. D. J. Brown: *Solid State Chem.* **115** (1995) 395.
- 20) V. M. Goldschmidt: *Ber. Dtsch. Chem. Ges.* **60** (1927) 1263 [in German].
- 21) V. M. Goldschmidt: *Fortschr. Min.* **15** (1931) 73 [in German].
- 22) F. S. Galasso: *Perovskites and High *t* Superconductors* (Gordon and Breach, New York, 1990).
- 23) V. Butler, C. R. A. Catlow, B. E. F. Fender, and J. H. Harding: *Solid State Ionics* **8** (1983) 109.
- 24) L. G. Tejuca, J. L. G. Fierro, and J. M. D. Tascon: *Adv. Catal.* **36** (1989) 385.
- 25) H. Yokokawa, N. Sakai, T. Kawada, and M. Dokiya: *Solid State Ionics* **52** (1992) 43.
- 26) N. W. Thomas: *Br. Ceram. Trans.* **96** (1997) 7.
- 27) R. D. Shannon and C. T. Prewitt: *Acta Crystallogr., Sect. B* **25** (1969) 925.
- 28) R. D. Shannon: *Acta Crystallogr., Sect. A* **32** (1976) 751.
- 29) S. C. Abrahams and J. L. Bernstein: *J. Chem. Phys.* **59** (1973) 1625.
- 30) B. Tell and H. M. Kasper: *Phys. Rev. B* **4** (1971) 4455.
- 31) A. N. Christensen and S. E. Rasmussen: *Acta Chem. Scand.* **19** (1965) 421.
- 32) I. V. Tananaev, D. F. Dzhurinskii, and Y. N. Mikhailov: *Zh. Neorgan. Khim.* **9** (1964) 1570 [in Russian].
- 33) L. Nyqvist and G. Johnsson: *Acta Chem. Scand.* **25** (1971) 1615.
- 34) P. Blaha, K. Schwarz, G. K. H. Madsen, D. Kvasnicka, and J. Luitz: *WIEN2K, An Augmented Plane Wave + Local Orbitals Program for Calculating Crystal Properties*, ed. K.-H. Schwarz (Tech. Universitat Wien, Vienna, 2001).
- 35) W. K. Chen, C. M. Cheng, J. Y. Huang, W. F. Hsieh, and T. Y. Tseng: *J. Phys. Chem. Solids* **61** (2000) 969.
- 36) S. K. Kurtz and T. T. Perry: *J. Appl. Phys.* **39** (1968) 3798.
- 37) J. P. Dougherty and S. K. Kurtz: *J. Appl. Crystallogr.* **9** (1976) 145.
- 38) R. W. Boyd: *Nonlinear Optics* (Academic Press, Boston, MA, 1992).
- 39) A. Graja: *Acta Phys. Pol. A* **37** (1970) 539.
- 40) P. N. Prasad and D. J. Williams: *Introduction to Nonlinear Optical Effects in Molecules and Polymers* (Wiley, New York, 1991) Chap. 6.
- 41) R. C. Eckardt, H. Masuda, Y. X. Fan, and R. L. Byer: *IEEE J. Quantum Electron.* **26** (1990) 922.